About the Art and Science of Visualizing Polymer Morphology using Transmission Electron Microscopy

Sylvie Tencé-Girault, Vincent Woehling, Evdokia Oikonomou, Szilvia Karpati, Sophie Norvez

About the Art and Science of Visualizing Polymer Morphology using Transmission Electron Microscopy

By: Sylvie Tencé-Girault,[a,*] Vincent Woehling, [a] Evdokia K Oikonomou, [a, ‡1] Szilvia Karpati [a, ‡2] and Sophie Norvez [a,*]

[a] Laboratoire Matière Molle et Chimie, ESPCI Paris, PSL Research University, 10 rue Vauquelin, 75005 Paris, France.

Abstract

Transmission electron microscopy is a unique tool to visualize polymer morphology, an intimate organization of the matter, encompassing crystalline features in semi-crystalline polymers and a kaleidoscopic collection of patterns produced by micro-separated phases in polymer blends. This manuscript aims at demonstrating the various opportunities this technique enables, through a miscellany of studies that have been performed in our laboratory. Materials as different as bulk and composite compounds, thin films, hollow fiber membranes, rubbers are presented, from the viewpoint of the interrelation of TEM with other techniques like scattering, mechanical and thermo-mechanical experiments.

‡1 Present address: Laboratoire Matière et Systèmes Complexes, UMR 7057 CNRS, Université Denis-Diderot Paris 7, Paris, France.

‡2 Present address: Laboratoire de Chimie, École Normale Supérieure de Lyon, 46 allée d'Italie 69364 Lyon Cedex 07, France.

Corresponding authors:

*sophie.norvez@espci.fr.; *sylvie.girault@espci.fr

Introduction

Exquisite and intriguing complex patterns provided by transmission electron microscopy (TEM) reveal secrets of polymer morphology.[1,2] Polymer morphology is an active area of research, aiming at understanding the properties of the end product or improving its processing.[3] Indeed, properties of polymeric materials (mechanical, thermal, optical, …) are to a considerable extent governed by morphological detail. [4-7] Morphology of polymers has its roots in either crystallization features, or macro/microphase separation, or even in a combination of both. Semi-crystalline polymers develop, either by cooling from a quiescent melt or after solvent evaporation, a hierarchical organization consisting of a crystal structure (0.1-1 nm, observable by WAXS (Wide Angle X-ray Scattering)), organized in lamellae (10-100 nm, accessible by SAXS (Small Angle X-ray Scattering), AFM (Atomic Force Microscopy) and TEM). The lamellae develop into microscopic superstructures, in particular spherulites (> 1000 nm, visible by optical microscopy or scanning electron microscopy (SEM)) consisting of crystalline layers radiating from the spherulite center.[8,9] Lamellar morphology is a periodic structure of crystalline and amorphous layers. Constituent chains participate to crystalline lamellae and amorphous phase, and when connecting at least two different crystalline lamellae, they contribute to the plastic and elastic behavior of semi-crystalline polymers.[10] Such a partial crystallization is due to the length of the flexible polymeric molecules that cannot disentangle from each other in the highly viscous melt. Since only a fraction of the polymer chains is transformed into crystals under such conditions of restraint, the crystallinity (volume or weight fraction of crystalline phase), rarely attains more that 50%.[8] Unlike most monomeric substances, polymer crystallization occurs under conditions far from equilibrium. Whereas the most stable state would be that of the fully extended chain, the crystals grow faster by chain folding.[8] On the other hand, morphological features (juxtaposition of phases different in nature) appear in blends of immiscible components. In this case, a macro- or microphase separation

appears, governed by the chemistry and the composition of the mixture (vide infra). As most of polymers are immiscible, a kaleidoscopic variety of morphologies may be obtained, furthermore extended in cases where amorphous and semi-crystalline polymers or copolymers are combined.

This fine organization unique to polymers became accessible to the research community some 60 years ago with the advent of commercial electron microscopes. A number of groups since then reported TEM observations of semi-crystalline polymers,[11-13] block copolymers,[14-16] or polymer blends.[17-19] TEM is however restricted to solid samples stable in the vacuum environment of the electron microscope. In parallel, cryo-electron microscopy was developed, allowing for the observation of frozen liquid samples. Winners of the 2017 Chemistry Nobel, Dubochet, Frank and Henderson shared the prize for developing techniques of biomolecules imaging.[20] More recently a liquid cell electron microscopy has emerged, when modern microfabrication techniques could build thin windows of silicon nitride with a controlled sub-micrometer separation, between which a liquid could be confined.[21] This new technique is well positioned to explore phenomena in evolution, e. g. nanomaterial growth, fluid physics or electrochemical processes. Deformation mechanisms may also be followed by *in-situ* TEM nano-mechanical testing. Hitherto restricted to hard materials, the technique has very recently been extended to polymeric samples.[22] Owing to significant instrumentation progresses over the last two decades, substantial advances have also been made in new stain-free imaging methods based either on phase contrast or on spectroscopic contrast.[23] As microphase-separated structures have become increasingly complicated with the development of controlled polymerization, three-dimensional imaging has also been of growing importance. Transmission electron microtomography (TEMT) is particularly useful when microphase separation of block copolymers produces interpenetrated three-dimensional morphologies.[24,25]

Besides, atomic force microscopy, which belongs to the family of scanning proximity probe microscopies developed since the late 1990s, has become a widely used technique that complements electron microscopy in studies of polymers.[26] AFM may provide direct real-space access on morphologies on all length scales of hierarchical ordering of polymers, and can be applied in a broad range of experimental conditions, including in liquid media, which renders the technique applicable for *in-situ* studies. In terms of ultimate resolution and tomographic capabilities, AFM cannot rival electron microscopy.[27] However, the technique is accurate enough to, for example, distinguish polymer backbone and side chains, or afford quantitative information about branching topology.[28]

Morphological studies based on indirect methods such as scattering, spectroscopic, calorimetric measurements interpret bulk behavior to deduce local polymer structure. In scattering experiments, a sample volume around 10^9 μm^3 is probed, in good adequacy with the macroscopic properties exhibited by the materials. However, because of the disorder and polydispersity inherent to polymeric materials, scattering signals are generally broad and multiple orders of diffraction are absent, rending somewhat difficult a precise interpretation of the spectra. Alternatively, TEM investigates a much smaller volume at the μm^3 scale, allowing for the examination of morphological details hidden in tiny domains. Even though TEM imaging can provide detailed information at levels down to atomic dimensions, such high resolution is hardly attainable in case of polymers. Indeed, on one hand polymers are sensitive to electron irradiation, and on the other hand, a poor contrast is expected from low atomic weight constituents of organic compounds. Nevertheless, since repetition scales in polymer morphologies are of the same order as the dimensions of the molecular coils (1-10 nm), TEM imaging provides, within this range, information which is relevant for these materials, that can rarely be obtained by other means.

TEM is thus an ultimate tool that comes to support hypotheses or models deduced from scattering techniques that give structural information. This microscope is like an eye in the heart of the matter, giving a direct view of polymer morphology, as soon as tricks inherent to the technique have been avoided. This manuscript aims at highlighting the wide power of this technique in the elucidation of polymer morphology, through a collection of studies that have been recently performed in our laboratory, though using a simple and conventional transmission electron microscope.[29] Materials as different as bulk compounds, thin films, hollow fiber membranes, rubbers are presented. It will be set forth, in particular, co-continuous structures in which two semi-crystalline polymers crystallize in domains as small as 10 nm, giving rise to improved optical and thermo-mechanical properties; nanocomposite structures in which carbon nanotubes act as nucleating agents for epitaxial crystallization of polyamide due to a fit of the cell parameters between both crystalline structures; how a triblock copolymer may act as a dispersing agent for carbon nanotubes, with the help of a selective solvent; how antifouling additives may be localized around the pores of hollow fiber membranes; how a block copolymer remains nanostructured in the constrained space of lamellar gallery of a semi-crystalline polymer, owing to the size of the nano-objects that fits the interlamellar distance.

Transmission electron microscopy and small-angle X-ray diffraction yield complementary results. TEM is also assisted by thermal or thermo-mechanical techniques to explain mechanical properties of polymer materials. Our studies are here reported from the viewpoint of interrelation among these techniques.

Discussion.

TEM is not such an easy-access technique, information about polymer morphology are obtained with various degrees of difficulty. Sample preparation and staining are crucial and highly skilled steps to obtain artifact-free imaging. When thin polymer films are interrogated, they may be

simply cast from solution onto microscopy grids covered with a carbon film. For solid samples however, ultrathin sections (40-60 nm) are required to be transparent to electrons. The sections must be carefully manufactured using ultra-microtomes, at a temperature below all glass transitions of the material to maintain the polymeric matter rigid enough during sectioning, most of the time around – 100 °C (ultra-cryo-microtomy). The cutting experimental conditions vary according to the materials chemistry, structure, morphology and geometry. Optimized protocols consisting in the delicate combination of the cutting temperature, speed and film thickness have to be developed for each system. In the case of fragile materials as porous fibers, inventive solutions must be found to preserve the integrity of samples. Here porous fibers were embedded in an Agar epoxy resin.[30] Specific problems as poor adhesion properties between the polymer and the resin had to be overcome at the microtomy step. Ultrathin sections are then transferred on a specific grid, using a glycerol drop. The nature of grids, copper or gold, depends on the staining agent that may oxidize copper. Selective staining is then applied to the material deposited on grids through contact with solutions (phosphotungstic acid (PTA)[31]) or vapors (OsO_4 or RuO_4)[32] of heavy metal salts or oxides. OsO_4 reacts with isolated double bonds (C=O, C=C), but not with conjugated double bonds.[18] RuO_4 does not react directly with chemical species, but rather forms clusters, staining most polymers but to a different degree dependent on the diffusion rate. RuO_4 diffuses preferably into the regions of lower density such as the amorphous regions of semi-crystalline polymers, staining them whereas the crystalline phase appears clearer.[18] The choice of the staining agent may result in a very different appearance of the same morphology. For instance Figure 1 shows the same morphology of a mixture of polyamide-6 (PA) with a PS-*b*-PBA-*b*-PS (polystyrene-polybutylacrylate-polystyrene) triblock copolymer.[33] In the left image, PA stained by PTA appears as black globules with sharp interfaces, while in the right image, RuO_4 stains preferentially the styrene block of the copolymer. Additional morphological details cover the PA globules that appear now in white.

This is one of the major tricks that should be considered with great care, in particular when measuring the sizes of the nano-objects by TEM. Such a dual staining may however be of particular interest to differentiate polymers of similar chemical composition, e. g. different acrylic blocks.[34]

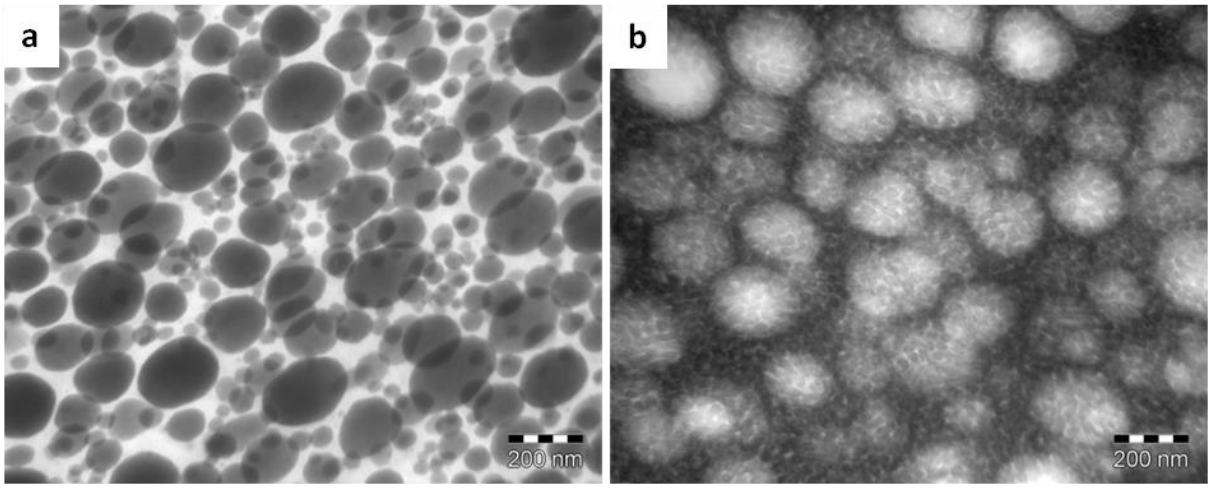

Figure 1. Co-extruded PA/PS-*b*-PBA-*b*-PS blend thin sections stained with a) Phosphotungstic acid; b) Ruthenium tetroxide.[33]

After this introduction on conditions to obtain valuable TEM images, we will discuss different polymer morphologies, first in relation with the juxtaposition of phases in blends of immiscible polymers, then with crystallization features in semi-crystalline polymers.

Polymer blending has long been considered as an efficient way to provide materials with improved properties.[35] In addition, blending represents an economical strategy that may bring significant cost reduction without substantial loss in properties, or improvement of the processability of some interesting polymers difficult to shape as neat. However, mixtures of polymers generally phase separate macroscopically, because the free energy of mixing is generally positive when mixing two long-chain polymers.[36] The free energy of mixing decomposes into an entropic and an energetic (enthalpic) part. The latter, reflected in the Flory interaction parameter χ, may promote mixing when χ negative. But generally, interactions

between components are of the van der Waals type, meaning that they are weak and repulsive, leading to a positive value of χ and to an enthalpic contribution opposing mixing. On the other hand, entropy always promotes mixing, but the gain is very little in case of long-chain polymer mixtures. Thus miscible polymer blends are very unlikely, unless specific interactions may occur between components (e. g. PMMA/PVDF mixtures, as it will be discussed later). This polymer immiscibility has been exploited to create materials with combination of improved mechanical, barrier, optical properties. Nevertheless, a key lies in the scale at which the components may structure. Block copolymers, in which immiscible blocks are covalently attached, exhibit local segregation of the blocks, yielding molecular-size structured objects. Such microphase-separated block copolymers combine at the nanometer scale the intrinsic properties of constituting homopolymers.[4] Self-assembly and morphology of block copolymers depend on their composition and architecture. Lamellae, hexagonally packed cylinders, bicontinuous gyroid or body-centered cubic structures are thermodynamically stable phases that have been observed.[37,38] The micro-phase separation is dictated by the degree of segregation, χN, where N is the total number of segments in the copolymer chain.[39,40] For diblock copolymers, lamellar phases are obtained when both blocks occupy equal volume fractions. With increasing asymmetric compositions, curved interfaces yield cylinders and then spheres. Architecture intervenes as an extra parameter for multiblock and graft copolymers.

Figure 2 shows SAXS and TEM observations recorded on a film made of a SBM triblock copolymer (polystyrene-*b*-polybutadiene-*b*-polymethylmethacrylate, $S_{16}B_{20}M_{64}$, M_n PS 11 k.mol^{-1}) containing 22 wt% of the parent SB diblock copolymer. The film was obtained by slow casting from $CHCl_3$, a good solvent for the three blocks of the copolymer.[41] The SAXS profile in Figure 2a exhibits three main peaks localized at q*, 2q* and 3q*, leading to a period d of 65 nm ($d = 2\pi/q^*$). As peaks are broad, we cannot exclude the existence of $\sqrt{2}q^*$ or $\sqrt{3}q^*$, and $\sqrt{7}q^*$signals characteristic of a cylinder organization. Whereas SAXS cannot allow to

differentiate lamellar or cylinder organization, TEM picture (Figure 2b) showing an end-on view of the cylinders brings an intimate image of the exact polymer morphology. In this picture, the characteristic distance between two cylinders is evaluated around 55 nm, in accordance with the SAXS profile. TEM observations provide another crucial information: the SB diblock is well incorporated in the SBM triblock microstructure, as no macrophase separation was observed. On the contrary such a phase separation between SBM and SB was previously observed in a SBM lamellar phase during annealing.[16]

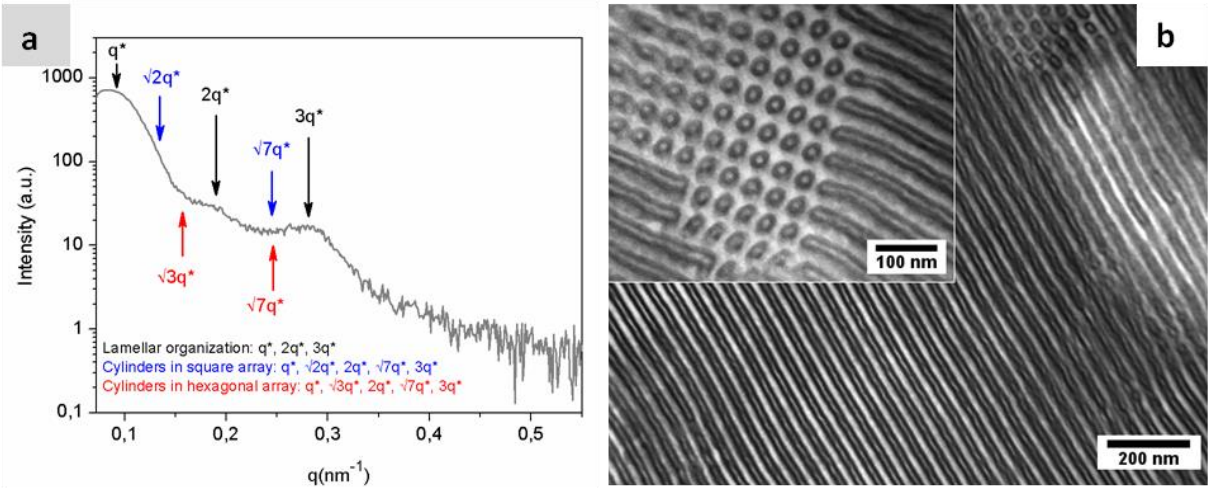

Figure 2. a) SAXS profiles of SBM films cast from $CHCl_3$ with three possible indexations: lamellae, cylinders in hexagonal or square array. b) Cylinder stacking of SBM observed by TEM. The B block is stained in black, the S block in light grey by OsO_4 vapor.[41]

The same SBM triblock copolymer was used, in combination with a solvent selective to one of the blocks, to homogeneously disperse carbon nanotubes (CNT).[41] Indeed, whereas chloroform is a good solvent for the three S, B and M blocks (interaction parameter χ around 0.0-0.3 for each), the situation is different with acetone, a poor solvent of S and B, χ = 0.4 and 1.0, respectively, but a good one for the M block. This unbalanced solubility induces curvature at the interface of the blocks, thereby allowing a better swelling of soluble chains, as

schematically depicted in Figure 3. When CNT are mixed with a chloroform or acetone solution of SBM (0.1 wt% CNT; ratio SBM/CNT: 3/1), they respectively aggregate or disperse homogeneously (Figure 3a,b). The blocks in poor solvent strongly adsorb onto the carbon nanotube surface to minimize their interaction with acetone, whereas the M block alone ensures the solubilization of the SBM. The polymer adsorbed onto the carbon surface entropically stabilizes the mixture, allowing for a homogeneous dispersion of the CNT. This situation which was only a hypothesis by observing the mixture in solution (Figure 3a,b) was proved by TEM (Figure 3c). One drop of the solution in acetone was deposited and evaporated onto a TEM carbon-coated copper grid, and stained by OsO_4 vapors. S and B blocks, marked in black, clearly appear located onto the surface of the nanotubes, owing to the solvophobic effect that is the driving force for the dispersion in acetone. Seen also in the TEM image are free "micelles" of SBM, namely SB cores surrounded by an M shell. Such stable suspensions were used to form master batches containing up to 25 wt% of CNT, easily dispersible into polymer matrices miscible with PMMA (e. g. PVDF [42]).

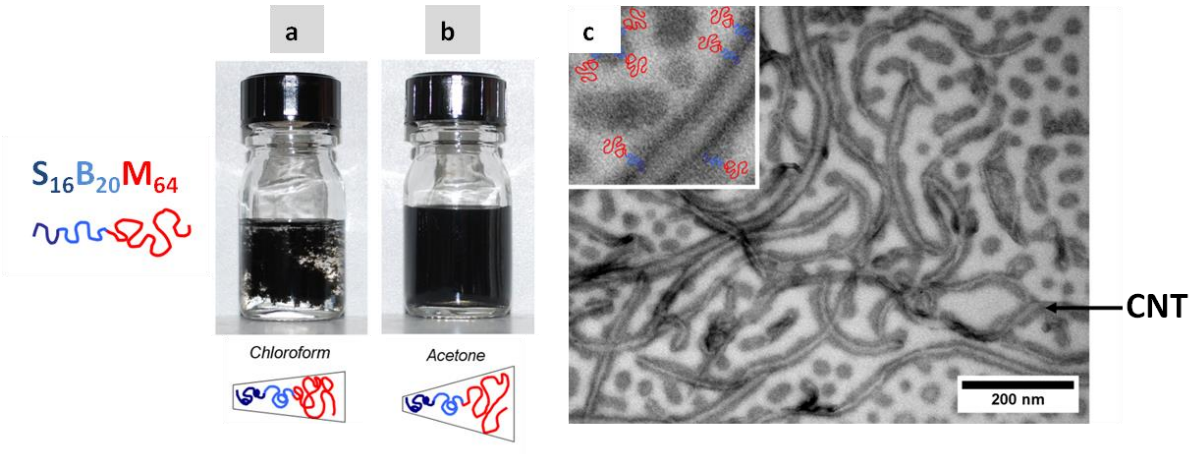

Figure 3. Vials containing SBM/CNT (3/1) in a) chloroform; b) acetone; Selective swelling of the SBM triblock is illustrated schematically. c) TEM image of a deposited drop of the SBM/CNT composite dispersed in acetone, stained with OsO_4. S and B appear in black.[41]

Apart from covalent attachment in multiblock copolymers, other strategies to prevent macrophase separation of immiscible polymers consist either in using interfacial agents also called compatibilizers, or in reactive blending.[43] Research on compatibilizers aiming at understanding and controlling the parameters relevant for blending has been widely developed in academic laboratories, whereas reactive blending is more attractive for industry. Generation of a copolymer in a one-shot process in continuous machines like extruders offers a simple and industrially scalable way to prepare stable polymer blends. Using a co-rotating twin-screw compounder at high temperatures, where all components are liquid and finely dispersed by the shearing, two functionalized and reactive homopolymers may react and organize at the molecular scale. The MAH (maleic anhydride)/NH_2 couple is commonly used for its high reactivity. MAH-functionalized polyethylene (FPE) and NH_2-terminated polyamide-6 (PA) blends containing 20% PA were reacted at high temperature in a twin-screw micro-compounder, giving rise to co-continuous structures.[6,44] These thermodynamically stable co-continuous nanostructured blends exhibit outstanding properties: transparency, excellent mechanical properties at low and high temperatures and solvent resistance. To understand the structure and properties of these blends, TEM (Figure 4a) proved to be a crucial experiment. While the crystallization of both components (FPE and PA) was demonstrated by thermal,[6,45] mechanical and diffraction analyses (WAXS, Figure 4b), the co-continuity was substantiated using TEM and solvent extraction experiments. Indeed, the co-continuous nanostructured organization presents a short-range order, no specific signal appears in SAXS experiment (Figure 4b). A well-defined peak appears only after alignment of the morphology after squeezing.[46] TEM image of Figure 4 was obtained from microtomed annealed extrudates cut perpendicularly to the flow direction, stained for 5 min at room temperature with an aqueous solution containing 2 wt% of phosphotungstic acid and 2 wt% of benzyl alcohol. In this TEM picture, the minority phase PA forms continuous domains appearing in black. The major phase,

light grey, corresponds to FPE. The characteristic size of the morphology, addition of the distance between PA domains ~ 60 nm and PA thickness ~ 15 nm is in agreement with the shoulder at 70 nm observed in the SAXS spectrum. In such a short-range order nanostructuration, TEM pictures were determinant to interpret SAXS data.

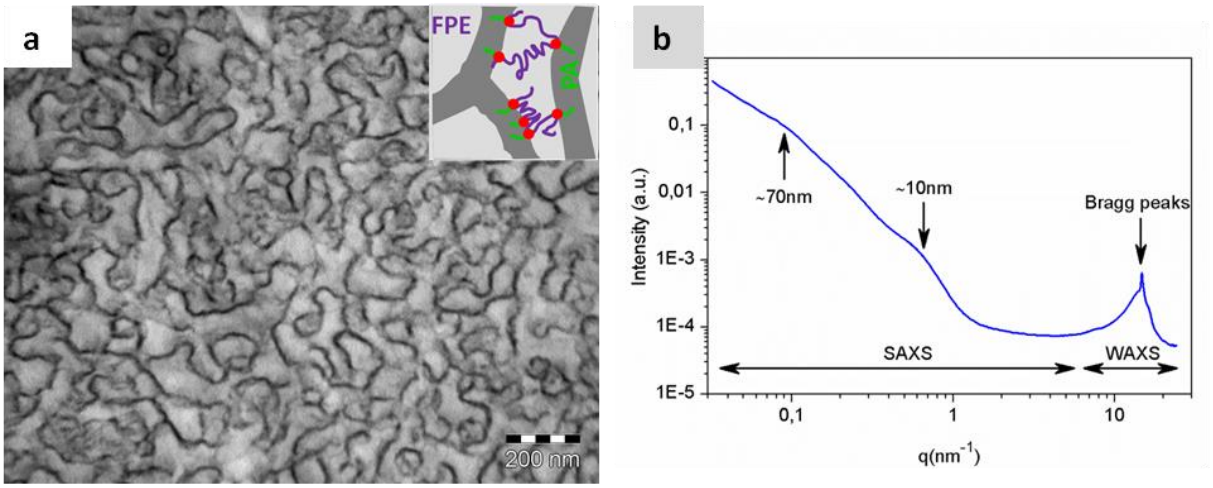

Figure 4. a) Co-continuous structure of FPE/PA blends with schematic FPE in purple and PA in green. b) X-ray diffraction spectrum showing no well-defined peak in the SAXS range (unless a broad peak associated to a crystalline and amorphous periodic organization of PA or FPE around 10 nm) and Bragg peaks in the WAXS range.

Nanostructured blends of PMMA and PA were also prepared by reactive blending.[47,48] The grafting reaction occurred between the amino end-group of PA and glutaric anhydride units randomly distributed along the backbone of PMMA. It was shown that short PA grafts facilitated reaction at the polymer interface during blending, whereas use of long PA chains led to macrophase separation and thereby poor mechanical properties. Nonetheless, by using triblock PMMA-PBA-PMMA copolymers instead of PMMA homopolymer, it was possible to efficiently graft long PA chains.[49] The higher efficiency of reactive blending in the case of triblock copolymer, compare to homopolymer, has been attributed to the ability of the ungrafted

triblock to mix with the grafted derivative formed during the blending process.[49] To understand the relationship between the position of reactive groups and the grafting efficiency (which thereby influences the mechanical properties), different acrylic architectures were synthesized by ATRP with a controlled distribution of the reactive groups.[33] For example, diblock copolymers composed of a first unreactive PBMA block (polybutylmethacrylate) and a second reactive PBMA block containing methacrylic acid monomers are schematized in Figure 5a (main PBMA chain in blue, the red spots indicating reactive acrylic acids define the second block of the copolymer. This second block is drawn in red in the insets of Fig. 5c and 5d). This strategy permitted tuning the grafting density by varying the length and the distribution of reactive functions in diblock and triblock copolymers.[33] By reactive blending in an extruder operated at 220 °C (speed 200 rpm, for 15 min under nitrogen atmosphere), NH_2-terminated PA chains (green chains in Figure 5) were grafted onto the COOH counterparts. For example, a symmetrical 50/50 unreacted diblock copolymer presents, right after extrusion, a spherical morphology, favored by the reacted block which imposes a curvature (Figure 5c). PA stained by phosphotungstic acid appears in black as 40-60 nm spheres. Annealing reveals that the morphology was not at equilibrium at the end of the blending process: after 24h at 235 °C (above the melting temperature of PA), the morphology has evolved toward the formation of vesicles. (Figure 5d). The sphere structure presents neither continuity nor bridges between PA domains: as seen in the DMA profile (Figure 5b), the mechanical properties of the blend are poor, and the material flows above 120 °C. After extrusion, the blend presents a higher storage modulus, and flows above 210 °C, the melting temperature of PA. The mechanical behavior of the blends is thus driven by crystallization of PA: before annealing, PA chains are distributed in small domains, which impedes crystallization. After annealing, the organization in multi-lamellar vesicles affords larger domains where PA can crystallize. Numerous PA chains can

incorporate these crystals, thereby connecting the PBMA backbones. The evolution of the mechanical behavior is hence explained by the morphology observed by TEM.

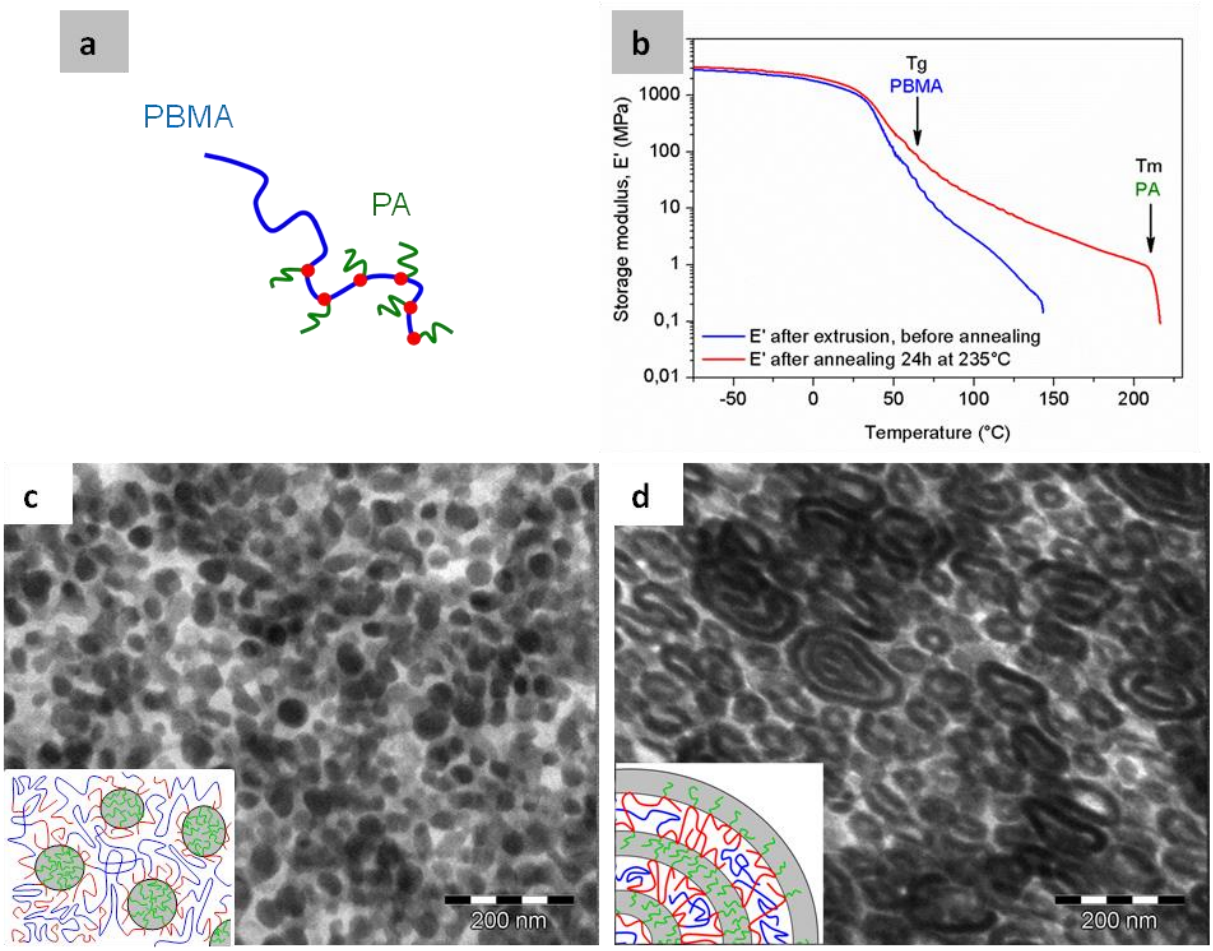

Figure 5. a) Schematic diblock PBMA-*b*-(PBMA-*g*-PA) copolymer. Length of the reactive block and grafting density may vary. b) Storage moduli E′ recorded in DMA before and after annealing [50] of a PBMA-*b*-(PBMA-*g*-PA) diblock copolymer, M_n 63k, 10 mol% reactive groups in the second block, M_n PA 2.5 kg.mol^{-1}. c) TEM image and sketch of the morphology before annealing. d) Morphology after annealing for 24h at 235 °C.

Reactive blending was also developed in the case of rubber mixtures, not with the use of extruders, but by competitive crosslinking after blending in an internal mixer. Our group reported that epoxidized natural rubber (ENR) could be efficiently cross linked by dicarboxylic

acids (Figure 6).[51-53] For instance, the curing of ENR25 (containing 25 wt% epoxy groups) with dodecanedioic acid is complete in 20 min at 180 °C. The crosslinking reaction occurs in bulk, through opening of the epoxy functions creating ester links along the chains. The resulting chemical network exhibits mechanical properties as good as the ones obtained when ENR is classically cross linked using sulfur or peroxides, in essence because such cross linked rubber preserves its capacity to crystallize under strain.[54] The reaction goes faster when the level of epoxidation increases. ENR50 is fully cross linked in 12 min, much quicker than ENR10. This difference in reactivity was exploited to quench the macrophase separation of the two immiscible ENR by competitive crosslinking.[55] By increasing the fraction of ENR50 in a mixture ENR10/ENR50, the resulting material switches from a soft rubber to a strong elastomer (Figure 7a). TEM explains this behavior: For 15% ENR50, nodules of ENR50 are dispersed in a soft matrix of non crosslinked ENR10 (Figure 7b), but above 37.5% ENR50, a co-continuous structure is obtained, in which ENR50 is cross linked while ENR10 is not (Figure 7c). Enlargement detailing a nodule of ENR50 (Figure 7d) shows crystalline features associated with the migration of the dicarboxylic acid crosslinker into the more reactive and polar ENR50.[56] Whereas depletion of the crosslinker in one phase was a drawback for reactive compatibilization, it turned out that the swelling of the more reactive phase by the curative was beneficial for the formation of a network. This opens the way to double networks of elastomers, since ENR10 is still available for crosslinking.

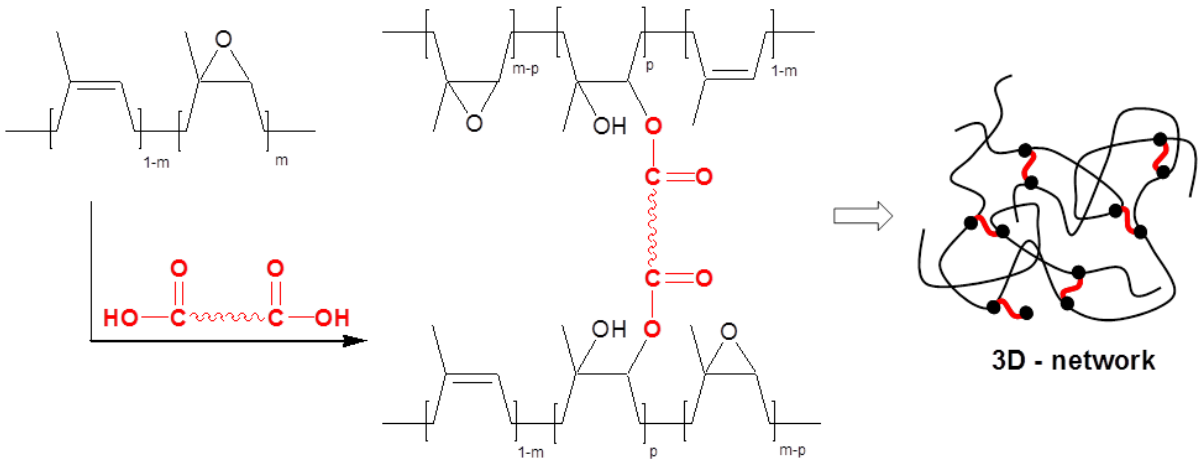

Figure 6. ENR crosslinking by dicarboxylic acids. For example, m = 0.25 for ENR25.

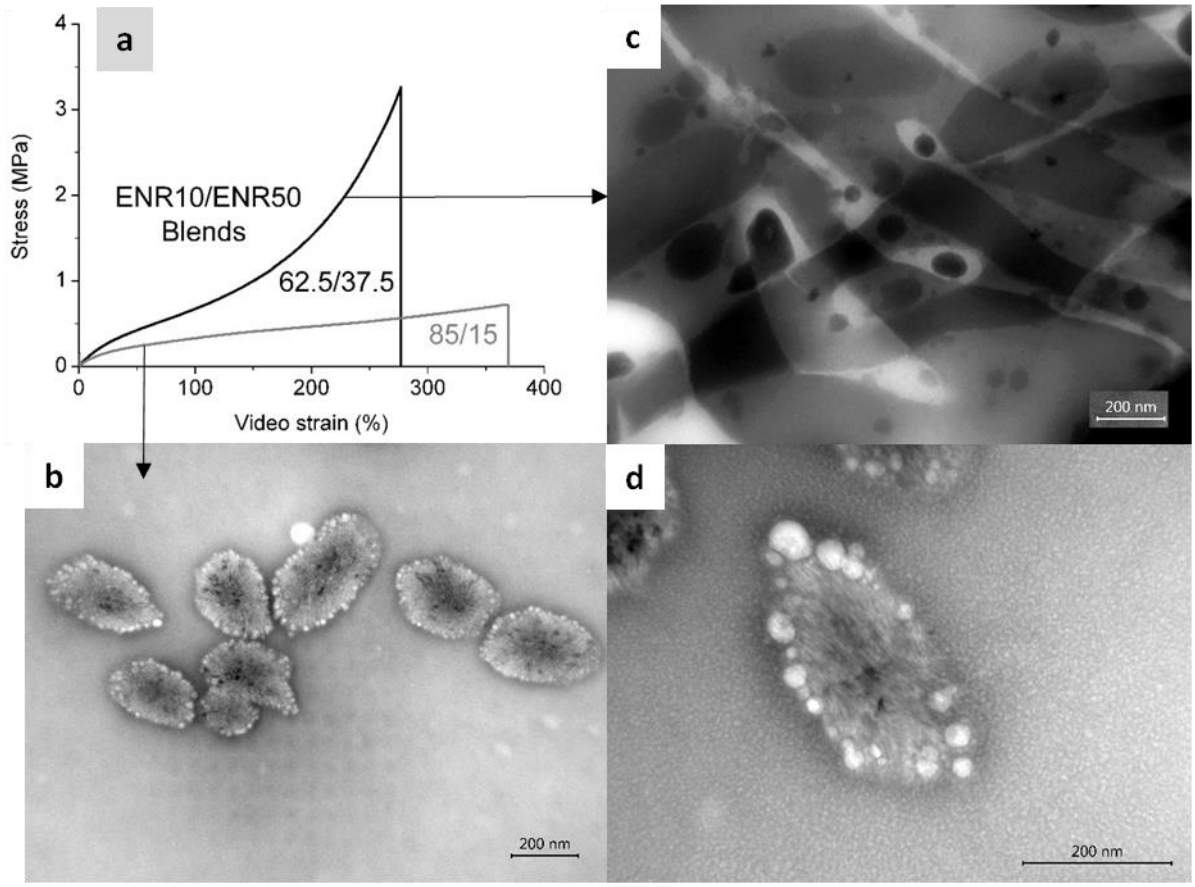

Figure 7. TEM pictures after curing of ENR50 blended with ENR10. Ultrathin sections prepared at – 100 °C were stained by an aqueous solution of phosphotungstic acid containing 2 wt% of benzyl alcohol, ENR50 containing more epoxy groups appears darker than ENR10. a) 37.5% ENR50 suffices to produce strong elastomeric properties. b) 85/15 sample, nodules

of ENR50 in soft ENR10 matrix. c) 62.5/37.5 sample, network of ENR50 in ENR10/ENR50 blend. d) 85/15 sample, higher magnification showing crystalline features inside nodules of ENR50.

TEM imaging also allows for the direct observation of low amounts of additives in a mixture. Antifouling additives have been widely used to improve the hydrophilic properties of porous membranes used for water purification. However, the exact localization of the active moieties in the porous matrices was never demonstrated before our group recently reported on the visualization of a polar biofouling agent in hollow fibers made of PVDF.[57] So far, only methods giving macroscopic information, as for example contact angle measurements, static protein adsorption or Raman spectroscopy[58] were available to attest hydrophilicity or fouling mitigation. Observation of the pore structure by transmission electron microscopy was made possible by embedding the fibers into a resin that filled in the voids and by specific staining of the antifouling additives. Figure 8 emphasizes the characterization of the porous system at different scales. The cryo-fractured hollow fiber shows a porous structure using a scanning electron microscope (Figure 8a,b). A large dispersion of pore size (0.1-10μm) is observed by SEM inside the fiber, the pore size is finely controlled only in the outer skin of the fiber (10-30 nm).[57] After embedding the delicate fiber in a resin, which permitted thin-sectioning, details of the pores were highlighted by TEM. Pores filled by the resin appear uniformly clear. The polar additive, polyvinylpyrrolidone, PVP, specifically stained in black by RuO_4 vapors (Figure 8c,d) appear darker all around the pores. This protocol for observing the localization of active additives in porous membranes is an efficient tool for the development of antifouling materials.

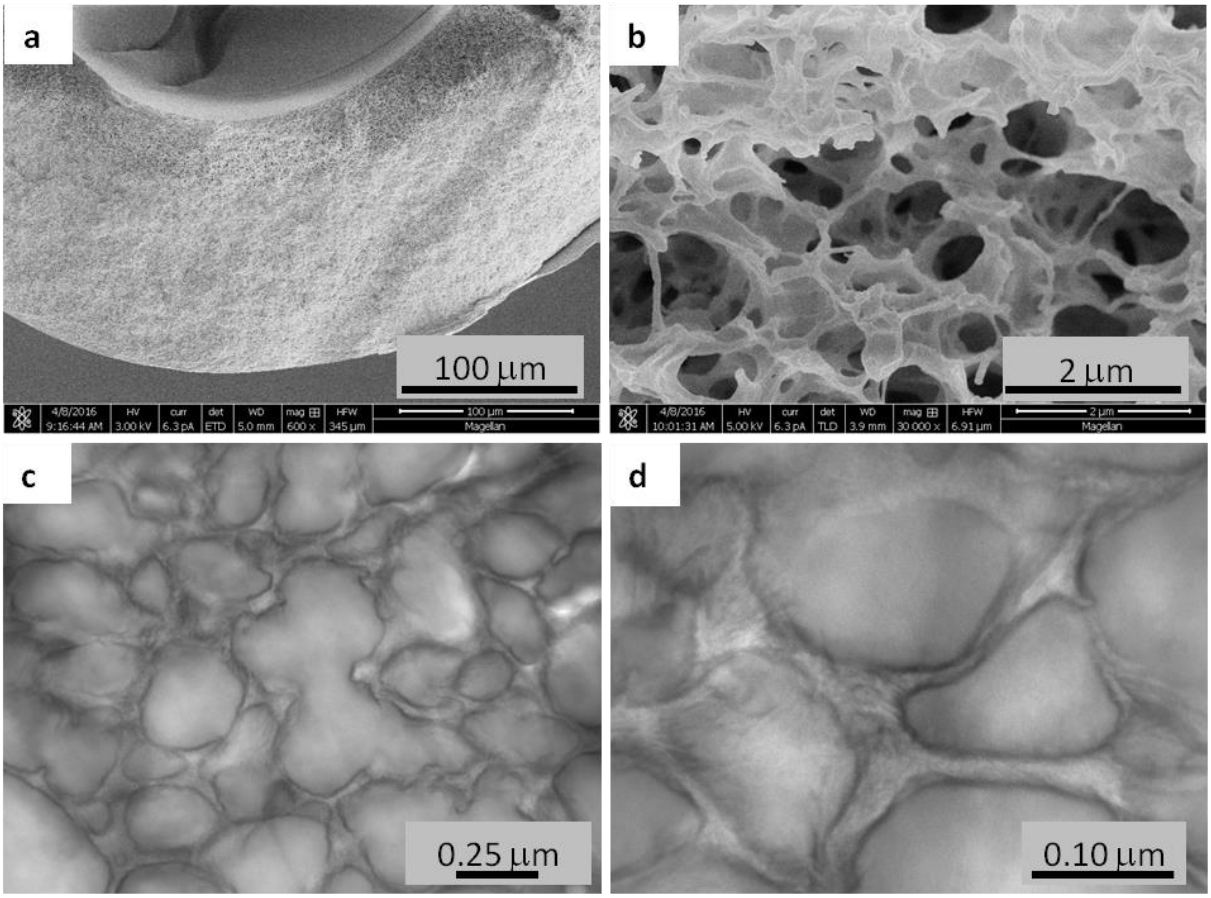

Figure 8. From macro to nano: a-b) Porous structure of a hollow fiber observed at different scales in scanning electron microscopy. c-d) The hydrophilic additive (PVP) decorating the very edge of the pores is revealed in black by TEM (fiber embedded in resin, RuO_4 staining).

Finally, we want to demonstrate through the two following examples that TEM is also a unique tool to observe how crystallization of a semi-crystalline polymer may be subtly affected by the presence of additives.

First consider the system where polyamide-6 (PA) was blended with increasing amounts of CNT (0-10%).[59] Non-isothermal crystallization from the melt observed by DSC is presented in Figure 9a. For neat PA, the crystallization peak presents a sharp maximum at 190 °C. With increasing amounts of well dispersed CNT, this peak broadens, shifts to higher temperatures and splits into two components. The temperature shift is more pronounced for peak 2, whose relative proportion increases with increasing CNT amount. At the crystallographic scale

explored by SAXS and WAXS, there were no differences that could explain the presence of this second crystallization peak.[59] The overall crystallinity was only slightly increased and no changes in cell parameters or lamellae period were observed. TEM only gave the answer, using staining with phosphotungstic acid and benzyl alcohol. Benzyl alcohol helps the diffusion of WO_3 in amorphous polyamide layers, thereby revealing a contrast between the stained amorphous domains and the crystalline lamellae of PA appearing whiter (Figure 9b). The splitting of the exothermic peak was thus assigned to morphological modifications: two types of lamellae stacks were formed, one for each peak of crystallization: lamellae independent of CNT in the matrix (visible in some parts of Figure 9c) and trans-crystalline lamellae growing perpendicularly to the CNT surfaces, with the polyamide chains parallel to the axis of the nanotubes (Figure 9d). This trans-crystalline lamellae formation is permitted by the crystallographic lattice of PA-6, which matches that of the graphitic hexagonal lattice of the carbon nanotube surface. This morphology is expected to have important consequences on the electrical properties of the composites, as the trans-crystalline polymer layer should behave as an insulating layer around the CNT.

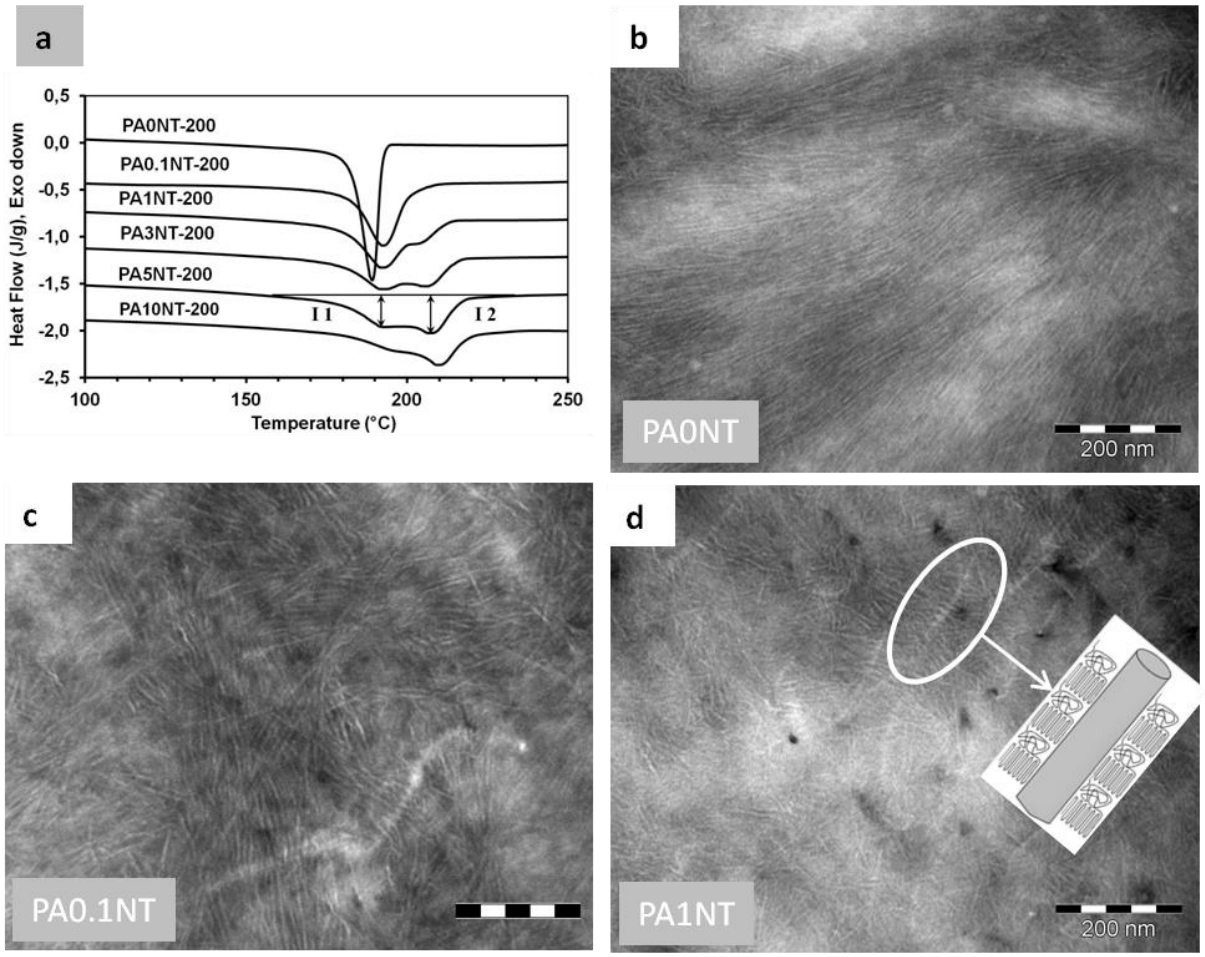

Figure 9. a) DSC cooling curves of PA/CNT composites at different CNT loadings.[59] b) Regular PA lamellae observed by TEM in neat PA. The PA amorphous phase is stained in black by PTA, while crystalline PA lamellae and CNT appear whiter. c)-d) TEM images showing the trans-crystalline lamellae in composites containing 0.1 and 1% CNT; in d) model for trans-crystallization of PA around the nanotubes.

In the second example, we explain by TEM why mechanical properties of semi-crystalline PVDF may be enhanced through intimate mixing with a nanostructured diblock copolymer.[60] The diblock copolymer (DB) is composed of a glassy PMMA block fully miscible with the amorphous part of PVDF and a soft acrylate block (PBA) which has no affinity for the PVDF. TEM image in Figure 10a shows that DB copolymer exhibits a nano-phase separation between blocks: domains of PBA (diameter ~ 6 nm), marked in black by RuO_4, appear dispersed

in the PMMA matrix. The average inter-domain distance is estimated at ~ 20 nm, in accordance with the SAXS profile of copolymer cast films, showing a unique characteristic distance at q ~ 0.27 nm^{-1} corresponding to a 23.5 nm distance (Figure 10a). SAXS experiments on PVDF/copolymer blends indicate a swelling of the crystalline/amorphous lamellar morphology. The long period L_p varies from 12 nm in pure PVDF to 20 nm in the presence of 25 wt% DB copolymer (Figure 10c). TEM reveals that the microphase-separated domains of the copolymer are confined into the amorphous lamellar gallery of PVDF. Figure 10b shows aligned micelles of DB, whose PBA core is specifically stained by RuO_4. This alignment highlights the crystalline lamellar organization of PVDF, which swells in accordance with DB content.[60] The copolymer can incorporate the amorphous phase between crystalline lamellae, and remained nano-structured, owing to the specific interactions between PMMA and PVDF components, and to the size of the micelles which is commensurable to the long period L_p of PVDF. Such a system, where the spherulitic lamellae of a semi-crystalline matrix integrates a nanostructured copolymer was new from an academic point of view, but also it yielded synergistically enhanced mechanical properties. Tensile tests demonstrated a 3-fold improvement of the elongation at rupture in presence of the copolymer, without significant loss of strength (Figure 10d). This break elongation improvement is likely related to the presence of the PBA block forming soft inclusions incorporated in the amorphous phase of PVDF, owing to miscible PMMA that serves to anchor PBA in PVDF matrix (Figure 10e).

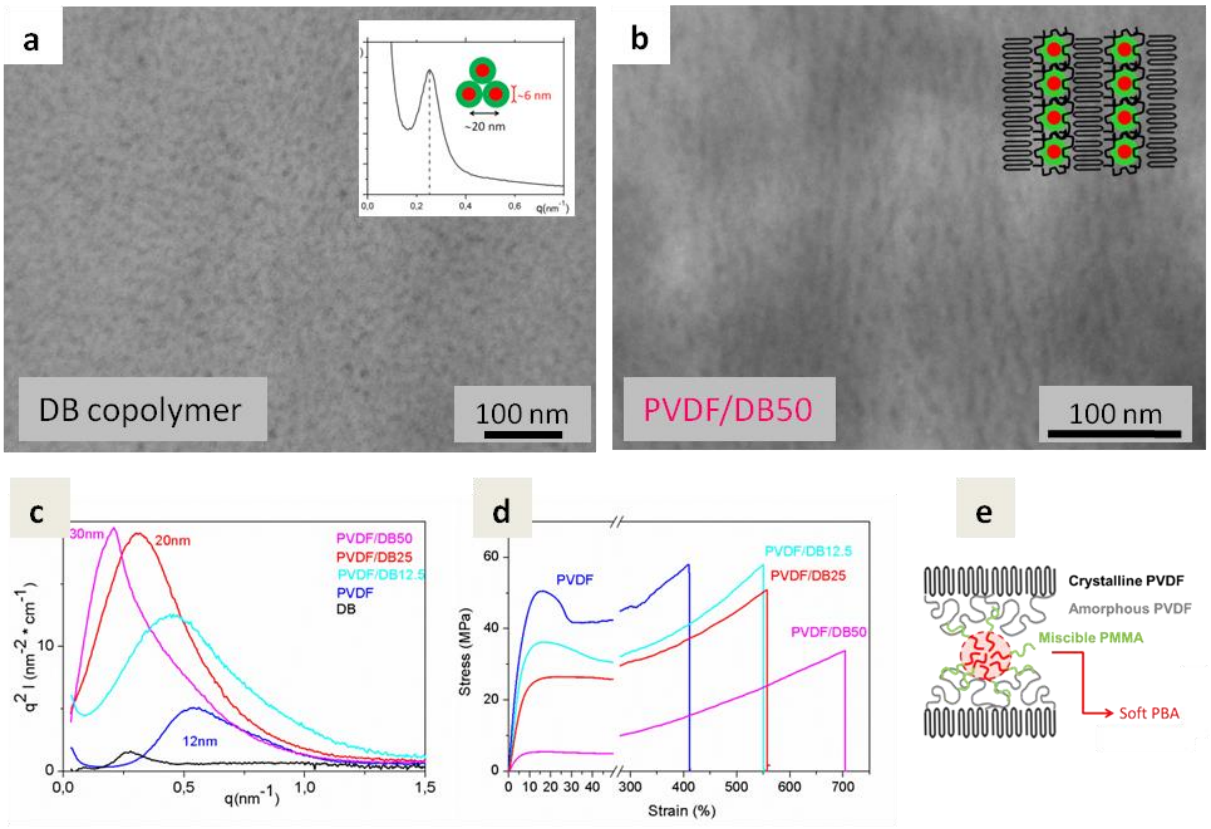

Figure 10. a) TEM image of DB copolymer; in insert: SAXS profile of neat diblock copolymer cast from NMP.[57] b) TEM image of blend PVDF containing 50% DB; micelles of DB whose PBA core is stained by RuO_4 appear in black; in insert: schematic micelles of copolymer incorporating the lamellar gallery of PVDF. c) SAXS signal of neat PVDF, DB and three PVDF/DB blends.[60] d) Stress-strain experiments comparing the three PVDF/DB blends with neat PVDF.[60] e) Schematic core-shell inclusion of the diblock copolymer in the crystalline/amorphous structure of PVDF.

Conclusion

Polymer morphology encompasses the crystalline features in semi-crystalline polymers and the luxuriant collection of patterns produced by macro- or micro-separated phases in polymer blends. TEM is one of the most powerful tool to understand the exact nature of the delicate inner organization of the polymeric matter. This manuscript aimed at demonstrating the various

opportunities that this technique enables. Our group also wishes to share his “know-how” of optimized protocols for cutting conditions and staining, acquired through preparation and observation of many samples presenting different morphologies linked to their chemical nature and structure. Our results were obtained using a simple transmission electron microscope. Beyond this conventional electron microscopy, the emerging techniques permitting observations in liquid cell or in-situ nano-mechanical experiments are expected in a near future to provide further informations, in particular about dynamic behavior of polymeric materials.

The morphological features are, to a considerable extent, under our control: we can shape them to our design. The strong efforts that have been made in the polymer community to characterize polymer morphology should further serve the development of new desirable properties and improved processes of manufacturing and recycling, as the ultimate goal of polymer morphology research should be the end product.

Acknowledgements

We are indebted to all PhD students and postdoctoral fellows who were major actors in all these studies: Anne-Carine Brosse, Gaëlle Carré de Lusancay, Séverin Dronet, Mathilde Freluche, Léa Gani, Cécile Gibon, Lucie Imbernon, Thomas Périé, Myriam Pire, and Cinzia Rotella. Arkema Group is sincerely thanked for financial support (A-C.B, S.D, M.F, L.G, C.G.), and for providing the CEM902 Zeiss electron microscope. Dr. Anne-Valérie Ruzette and Patrick Coupard (Arkema) who initiated the first TEM observations in our laboratory are sincerely thanked for training and kind sharing of their expertise. Dr. Ilias Iliopoulos is warmly acknowledged for fruitful discussions and his continuous and true support.

Table of Contents

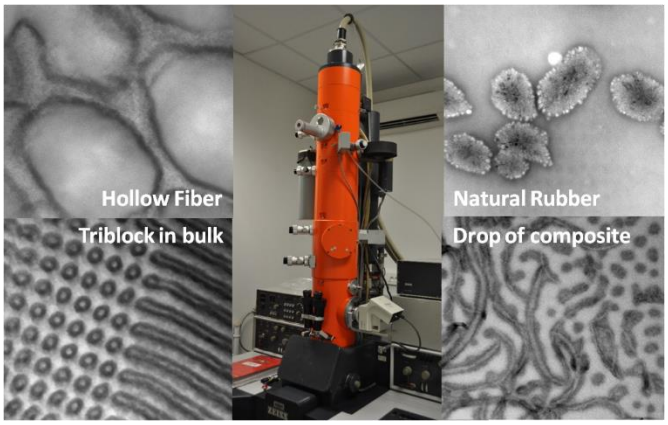

Polymer morphology, which encompasses a luxuriant collection of patterns produced by micro-separated phases in polymer blends, composites, or semi-crystalline polymers, has a crucial impact on the macroscopic properties of these materials. Transmission electron microscopy is a unique tool to investigate these intimate organizations, in interrelation with scattering and thermo-mechanical experiments.

[1] G. H. Michler, *Electron Microscopy of Polymers*, Springer, 2010.

[2] L. C. Saywer, D. T. Grubb, G. F. Meyers, *Polymer microscopy*, 3rd ed.; Springer: New York, 2008.

[3] Q. Guo, *Polymer Morphology: Principles, Characterization, and Processing*, Wiley, 2016.

[4] A. V. Ruzette, L. Leibler, Block copolymers in tomorrow's plastics, *Nature Materials* **2005**, *4*, 19–31.

[5] L. Corté, F. Beaume, L. Leibler, Crystalline organization and toughening: example of polyamide-12, *Polymer* **2005**, *46*, 2748–2757.

[6] H. Pernot, M. Baumert, F. Court, L. Leibler, Design and properties of co-continuous nanostructured polymers by reactive blending, *Nature Materials* **2002**, *1*, 54–58.

[7] M. C. Orilall, U. Wiesner, Block copolymer based composition and morphology control in nanostructured hybrid materials for energy conversion and storage: solar cells, batteries, and fuel cells, *Chem. Soc. Rev.* **2011**, *40*, 520–535.

[8] J. M. Schultz, *Polymer Crystallization - The development of Crystalline Order in thermoplastic Polymers*; American Chemical Society Washington D.C., Oxford University Press, 2001.

[9] J. M. Schultz, Self-generated fields and polymer crystallization, *Macromolecules* **2012**, *45*, 6299–6323.

[10] S. Jabbari-Farouji, O. Lame, M. Perez, J. Rottler, J.-L. Barrat, Role of the Intercrystalline Tie Chains Network in the Mechanical Response of Semicrystalline Polymers, *PRL* **2017**, *118*, 217802.

[11] H. Sano, T. Usami, H. Nakagawa, Lamellar morphologies of melt-crystallized polyethylene, isotactic polypropylene and ethylene-propylene copolymers by the $Ru0_4$ staining technique, *Polymer* **1986**, *27*, 1497–1504.

[12] R. V. Castillo, A. J. Müller, Crystallization and morphology of biodegradable or biostable single and double crystalline block copolymers, *Prog. Polym. Sci.* **2009**, *34*, 516–560.

[13] S. Nojima, Y. Akutsu, A. Washino, S. Tanimoto, Morphology of melt-quenched poly(3-caprolactone)-block-polyethylene Copolymers, *Polymer* **2004**, *45*, 7317–7324.

[14] S. Sakurai, T. Momii, K. Taie, M. Shibayama, S. Nomura, Morphology Transition from Cylindrical to Lamellar Microdomains of Block Copolymers, *Macromolecules* **1993**, *26*, 485–491.

[15] R. Stadler, C. Auschra, J. Beckmann, U. Krappe, I. Voigt-Martin, L. Leibler, Morphology and Thermodynamics of Symmetric Poly(A-block-B-block-C) Triblock Copolymers, *Macromolecules* **1995**, *28*, 3080–3097.

[16] L. Corté, K. Yamauchi, F. Court, M. Cloître, T. Hashimoto, L. Leibler, Annealing and Defect Trapping in Lamellar Phases of Triblock Terpolymers, *Macromolecules* **2003**, *36*, 7695–7706.

[17] V. Abetz, P. F. W. Simon, Phase Behaviour and Morphologies of Block Copolymers, *Adv. Polym. Sci.* **2005**, *189*, 125–212.

[18] T. Inoue, in: *Polymer Blend Handbook*, Chap. 8: Morphology of Polymer Blends, 2003.

[19] M. Radjabian, C. Abetz, B. Fischer, A. Meyer, B. Lademann, V. Abetz, Structure Formation of Binary Blends of Amphiphilic Block Copolymers in Solution and in Bulk, *Macromol. Chem. Phys.* **2017**, *218*, 1600587.

[20] E. Callaway, *Nature* **2017**, *550*, 167.

[21] F. M. Ross, Opportunities and challenges in liquid cell electron microscopy, *Science* **2015**, *350* issue 6267, p. 1490, DOI: 10.1126/science.aaa9886

[22] N. Velez, F. Allen, M.-A. Jones, G. Meyers, A. M. Minor, Development of Quantitative In Situ TEM Nanomechanical Testing for Polymers, *Microsc. Microanal.* **2017**, *23* (Suppl 1), 742–743.

[23] M. R. Libera, R. F. Egerton, Advances in the Transmission Electron Microscopy of Polymers, *Polym. Rev.* **2010**, *50*, 321–339.

[24] H. Jinnai, R. J. Spontak, Transmission electron microtomography in polymer research, *Polymer* **2009**, *50*, 1067–1087.

[25] H. Jinnai, T. Higuchi, X. Zhuge, A. Kumamoto, K. J. Batenburg, Y. Ikuhara, Three-Dimensional Visualization and Characterization of Polymeric Self-Assemblies by Transmission Electron Microtomography, *Acc. Chem. Res.* **2017**, *50*, 1293−1302.

[26] H. Schönherr, G. J. Vancso, *Scanning Force Microscopy of Polymers*, Springer, 2010.

[27] Reference 3, Chap. 6.

[28] S. Y. Yu-Su, F. C. Sun, S. S. Sheiko, D. Konkolewicz, H.-i Lee, K. Matyjaszewski, Molecular Imaging and Analysis of Branching Topology in Polyacrylates by Atomic Force Microscopy, *Macromolecules* **2011**, *44*, 5928–5936.

[29] All polymer morphologies shown in this manuscript were observed using a CEM902 Zeiss microscope operating under a voltage acceleration of 80 kV.

[30] Fibers were placed for 1h in a mold containing the Agar resin (4.8 g of LV Resin, 1.6 g of VH1 Hardener, 3.6 g of VH2 Hardener and 0.25 g of accelerator), at room temperature under dynamic vacuum, to fill in the fiber pores. Then, the mold was placed at 70 °C for 15h to harden the resin. For ultra-cryo-microtomy, the cutting speed varied in the range of 0.4 to 1 $mm.s^{-1}$.

[31] TEM copper grids bearing the thin sections were floated for 10-30 min at a chosen temperature onto a 2 wt% aqueous solution of $H_3PO_4.12WO_3$ (PTA) and benzyl alcohol, then on a water drop for rinsing.

[32] Vapor phase deposition: grids were held above a vial containing the staining solution: aqueous solution of RuO_4 (2 wt%, for 1-5 min) or OsO_4 (4 wt%, for ~ 30 min), no rinsing step.

[33] S. Dronet, PhD Thesis, Matériaux nanostructurés obtenus par combinaison de polymérisation radicalaire contrôlée et mélangeage réactif, Pierre-et-Marie-Curie University, **2009**, Paris, France.

[34] A. V. Ruzette, S. Tencé-Girault, L. Leibler, F. Chauvin, D. Bertin, O. Guerret, P. Gérard, Molecular Disorder and Mesoscopic Order in Polydisperse Acrylic Block Copolymers Prepared by Controlled Radical Polymerization, *Macromolecules* **2006,** *39,* 5804–5814.

[35] J. W. Barlow, D. R. Paul, H. Keskkula, in: *Polymer blends in Encyclopedia of Polymer Science and Engineering* 2nd Ed. Vol. 12, 399–461 (Wiley, New York, 1988).

[36] M. Rubinstein, R. H. Colby, *Polymer Physics*, Oxford University Press, 2003.

[37] Y. Mai, A. Eisenberg, Self-assembly of block copolymers, *Chem. Soc. Rev.* **2012**, *41*, 5969–5985.

[38] A. K. Khandpur, S. Forster, F. S. Bates, I. W. Hamley, A. J. Ryan, W. Bras, K. Almdal, K. Mortensen, Polyisoprene-Polystyrene Diblock Copolymer Phase Diagram near the Order-Disorder Transition, *Macromolecules* **1995,** *28***,** 8796–8806.

[39] L. Leibler, Theory of Microphase Separation in Block Copolymers, *Macromolecules* **1980**, *13*, 1602–1617.

[40] M. W. Matsen, F. S. Bates, Unifying Weak- and Strong-Segregation Block Copolymer Theories, *Macromolecules* **1996**, *29*, 1091–1098.

[41] T. Périé, A.-C. Brosse, S. Tencé-Girault, L. Leibler, Nanostructured films and composites from carbon nanotubes dispersed by ABC block terpolymers in selective solvent, *Polymer* **2011**, *52*, 3065–3073.

[42] C. M. Gibon, S. Norvez, S. Tencé-Girault, J. T. Goldbach, *Macromolecules* **2008**, *41*, 5744–5752.

[43] C. Koning, M. Van Duin, C. Pagnoulle, R. Jerome, Strategies for Compatibilization of Polymer Blends, *Prog. Polym. Sci.* **1998**, *23*, 707–757.

[44] L. Gani, S. Tencé-Girault, M. Milléquant, S. Bizet, L. Leibler, Co-continuous Nanostructured Blend by Reactive Blending: Incorporation of High Molecular Weight Polymers, *Macromol. Chem. Phys.* **2010**, *211*, 736–743.

[45] M. E. Córdova, A. T. Lorenzo, A. J. Müller, L. Gani, S. Tencé-Girault, L. Leibler, The Influence of Blend Morphology (Co-Continuous or Sub-Micrometer Droplets Dispersions) on the Nucleation and Crystallization Kinetics of Double Crystalline Polyethylene/Polyamide Blends Prepared by Reactive Extrusion, *Macromol. Chem. Phys.* **2011**, *212*, 1335–1350.

[46] C. Rotella, S. Tencé-Girault, M. Cloître, L. Leibler, Shear-induced Orientation of Cocontinuous Nanostructured Polymer Blends, *Macromolecules* **2014***, 47*, 4805–4812.

[47] M. Freluche, I. Iliopoulos, J. J. Flat, A. V. Ruzette, L. Leibler, Self-organized materials and graft copolymers of polymethylmethacrylate and polyamide-6 obtained by reactive blending, *Polymer* **2005**, *46*, 6554–6562.

[48] M. Freluche, I. Iliopoulos, M. Milléquant, J.-J. Flat, L. Leibler, Graft Copolymers of Poly(methyl methacrylate) and Polyamide-6: Synthesis by Reactive Blending and Characterization, *Macromolecules* **2006**, *39*, 6905-6912.

[49] I. Iliopoulos, L. Leibler, M. Freluche, J.-J. Flat, P. Gerard, Glassy-Crystalline Nanostructured Polymers Via Reactive Blending, *Macromol. Symp.* **2006**, *245–246*, 371–374.

[50] DMA curves of PBMA-*b*-(PBMA-*g*-PA) copolymers were obtained by a mechanical analyzer from TA Instruments (DMA2980). Rectangular bars were tested in tension film mode. A sample oscillatory deformation of 0.1% was applied at 1 Hz. Samples were cooled down to low temperatures (– 80 °C) then the evolution of storage (E') and loss (E") Young moduli were recorded upon heating at 2 °C.min^{-1} up to 250 °C.[33]

[51] M. Pire, S. Norvez, I. Iliopoulos, B. Le Rossignol, L. Leibler, Epoxidized natural rubber/dicarboxylic acid self-vulcanized blends, *Polymer* **2010**, *51*, 5903–5909.

[52] M. Pire, S. Norvez, I. Iliopoulos, B. Le Rossignol, L. Leibler, Imidazole-promoted acceleration of crosslinking in epoxidized natural rubber/dicarboxylic acid blends, *Polymer* **2011***, 52*, 5243–5249.

[53] M. Pire, C. Lorthioir, E. K. Oikonomou, S. Norvez, I. Iliopoulos, B. Le Rossignol, L. Leibler, Imidazole-accelerated crosslinking of epoxidized natural rubber by dicarboxylic acids: a mechanistic investigation using NMR spectroscopy, *Polym. Chem.* **2012**, *3*, 946–953.

[54] L. Imbernon, R. Pauchet, M. Pire, P.-A. Albouy, S. Tencé-Girault, S. Norvez, Strain-induced crystallization in sustainably crosslinked epoxidized natural rubber, *Polymer* **2016**, *93*, 189–197.

[55] L. Imbernon, M. Pire, E. K. Oikonomou, S. Norvez, Semi-interpenetrating Networks in Blends of Epoxidized Natural Rubbers, *Macromol. Chem. Phys.* **2013**, *214*, 806–811.

[56] L. Imbernon PhD Thesis. Réticulation non-permanente, physique ou chimique, du caoutchouc naturel époxydé. Propriétés dynamiques et recyclage, Pierre-et-Marie-Curie University, Paris, 2015.

[57] E. K. Oikonomou, S. Karpati, S. Gassara, A. Deratani, F. Beaume, O. Lorain, S. Tencé-Girault, S. Norvez, Localization of antifouling surface additives in the pore structure of hollow fiber PVDF membranes, *J. Memb. Sci.* **2017**, *538*, 77–85.

[58] E. Dufour, S. Gassara, E. Petit, C. Pochat-Bohatier, A. Deratani, Quantitative PVP mapping in PVDF hollow fiber membranes by using Raman spectroscopy coupled with spectral chemiometrics analysis, *Eur. Phys. J. Spec. Top.* **2015**, *224*, 1911–1919.

[59] A.-C. Brosse, S. Tencé-Girault, P. M. Piccione, L. Leibler, Effect of multi-walled carbon nanotubes on the lamellae morphology of polyamide-6, *Polymer* **2008**, *49*, 4680–4686.

[60] E. K. Oikonomou, S. Tencé-Girault, P. Gérard, S. Norvez, Swelling of semi-crystalline PVDF by a PMMA-based nanostructured diblock copolymer: Morphology and mechanical properties, *Polymer* **2015**, *76*, 89–97.